

Article

Comparison of Advanced Oxidation Processes for the Degradation of Maprotiline in Water—Kinetics, Degradation Products and Potential Ecotoxicity

Nuno P. F. Gonçalves ^{1,*} , Zsuzsanna Varga ², Edith Nicol ² , Paola Calza ¹ and Stéphane Bouchonnet ²¹ Department of Chemistry, University of Turin, 10124 Torino, Italy; Paola.calza@unito.it² Laboratoire de Chimie Moléculaire, CNRS/Ecole Polytechnique, Institut Polytechnique de Paris, 91128 Palaiseau, France; zsuzsanna.varga@polytechnique.edu (Z.V.); edith.nicol@polytechnique.edu (E.N.); stephane.bouchonnet@polytechnique.edu (S.B.)

* Correspondence: nunopaulo.ferreiragoncalves@unito.it

Abstract: The impact of different oxidation processes on the maprotiline degradation pathways was investigated by liquid chromatography-high resolution mass spectrometry (LC/HRMS) experiments. The in-house SPIX software was used to process HRMS data allowing to ensure the potential singular species formed. Semiconductors photocatalysts, namely Fe-ZnO, Ce-ZnO and TiO₂, proved to be more efficient than heterogeneous photo-Fenton processes in the presence of hydrogen peroxide and persulfate. No significant differences were observed in the degradation pathways in the presence of photocatalysis, while the SO₄[−] mediated process promote the formation of different transformation products (TPs). Species resulting from ring-openings were observed with higher persistence in the presence of SO₄[−]. In-silico tests on mutagenicity, developmental/reproductive toxicity, Fathead minnow LC₅₀, D. magna LC₅₀, fish acute LC₅₀ were carried out to estimate the toxicity of the identified transformation products. Low toxicant properties were estimated for TPs resulting from hydroxylation onto bridge rather than onto aromatic rings, as well as those resulting from the ring-opening.

Keywords: maprotiline; advanced oxidation processes; LC/HRMS coupling; structural elucidation; kinetics; ecotoxicity estimations



Citation: Gonçalves, N.P.F.; Varga, Z.; Nicol, E.; Calza, P.; Bouchonnet, S. Comparison of Advanced Oxidation Processes for the Degradation of Maprotiline in Water—Kinetics, Degradation Products and Potential Ecotoxicity. *Catalysts* **2021**, *11*, 240. <https://doi.org/10.3390/catal11020240>

Academic Editors: Stephanie Lambert and Julien Mahy

Received: 13 January 2021

Accepted: 8 February 2021

Published: 11 February 2021

Publisher's Note: MDPI stays neutral with regard to jurisdictional claims in published maps and institutional affiliations.



Copyright: © 2021 by the authors. Licensee MDPI, Basel, Switzerland. This article is an open access article distributed under the terms and conditions of the Creative Commons Attribution (CC BY) license (<https://creativecommons.org/licenses/by/4.0/>).

1. Introduction

A consequence of human activities is the arising of so-called contaminants of emerging concern (CECs) and their subsequent detection in surface-, ground-, and drinking water worldwide [1–3]. Particular attention should be paid to compounds that are scarcely biodegradable, such as pharmaceuticals, personal care products, hormones, food additives, artificial sweeteners, pesticides, and dyes among others [4–6]. Due to their distinct chemical properties (polarity, functional groups, solubility, . . .) and potential persistence, CECs are poorly removed by conventional wastewater treatment methodologies and are thus frequently detected in the wastewater treatment plant (WWTP) effluents [7]. These effluents act as a constant low-level source of such substances to the environment. For example, antidepressants and psychotic drugs, as a result of their fast increasing consumption [8,9] and high stability, have been recently observed in surface water and wastewater [10]. Their environmental hazardousness is not related to their (usually low) concentrations, but to their continuous discharge, persistence, and high biological activity [11]. Like many other pharmaceuticals, antidepressants may be excreted in their native form or as metabolites and enter the water bodies via different pathways. This class of drugs is of particular concern as it affects not only the central nervous system but also the reproduction, growth, and immune functions [12,13]. Moreover, tricyclic and tetracyclic antidepressants are known to have several side-effects when consumed by humans and their exposure to

fish increased mortality, developmental retardation, and morphological anomalies [12]. Maprotiline is a tetracyclic antidepressant drug with fast-growing consumption that has been detected in surface water and wastewater at $\mu\text{g L}^{-1}$ concentrations [14,15]. A study monitoring pharmaceuticals in the Baltic Sea region [16] detected maprotiline in around 50% of influents and effluents wastewater treatment plants with only 44% of removal by the conventional wastewater treatment methodologies. Alarming, the study also reports significant bioaccumulation with a concentration of more than 170 $\mu\text{g/kg}$ of maprotiline in blue mussels in the same region.

Advanced oxidation processes (AOPs) have emerged as a promising approach to efficiently remove a wide range of recalcitrant pollutants by reaction with generated strong radical oxidants (mostly hydroxyl radical $\bullet\text{OH}$ and sulfate radical $\text{SO}_4^{\bullet-}$) [17]. Among AOPs, heterogeneous photocatalysis processes demonstrated to be efficient in achieving the degradation and in most cases the mineralization of a wide range of pollutants [18–20]. TiO_2 and ZnO materials have been extensively investigated for water treatment because they are non-toxic, chemically, and biologically inert, inexpensive and they have a high capability to generate reactive species [21–24]. The introduction of doping agents in the reticular structure of zinc oxide materials is described to reduce the charge recombination increasing in this way the photocatalytic efficiency [23,25]. In previous studies, we demonstrated that the addition of iron [26] and cerium [27] in proper amounts promote interesting photocatalytic properties, increasing the removal efficiency of water pollutants.

Other AOPs, widely investigated due to their high effectiveness, are based on (photo)-Fenton-like processes, characterized by the formation of reactive species mediated by iron. The use of an iron-based heterogeneous catalyst allows the catalyst recovery and reusability with a low amount of iron released in solution, thus avoiding sludge formation and simplifying the process in comparison with the conventional homogeneous process [18]. In previous studies, we demonstrated that the stabilization of Fe(II) ions in the magnetite structure, essential to keep the system active, can be achieved by coating them with humic acid substances [28]. The use of magnetite particles coated with humic acid ($\text{Fe}_3\text{O}_4/\text{HA}$) as catalysts for heterogeneous (photo)-Fenton processes, proved to effectively activate hydrogen peroxide and persulfate, for the degradation of pollutants in water [28,29].

Despite the efficiency of some oxidation technologies, many questions remain about pollutant degradation pathways. The generated transformation products (TPs) can be even more toxic and persistent than the parent molecule itself. For example, relatively safe pharmaceuticals, such as ibuprofen and naproxen are described to form TPs that are many times more toxic than the parent compound [30,31]. Sinclair et al., analyzing the toxicity of hundreds of TPs formed from the degradation of several synthetic chemicals, reported that even if the majority were less or presented similar toxicity of the parent molecule, 20% were >3 times more toxic and 9% were >10 times more toxic than the parent compound [32]. Thus, it is important not only to degrade the parent molecule, but also to study the degradation products and ideally achieve their mineralization [33–35].

In a previous study, maprotiline degradation in river water proved to occur through the formation of 12 intermediates resulting from hydroxylation/oxidation and ring-opening [36]. Conversely, photocatalytic experiments proved to lead to more complex degradation pathways with the formation of a significantly higher number of TPs, resulting mainly from the drug multi-hydroxylation. Moreover, by retrospective analysis of wastewater effluents samples, we ascertained that several of these species are also formed during the wastewater treatment processes, thus being released into the environment. This fact raises concerns about how the wastewater oxidation processes can impact the degradation pathways and consequently the toxicity of the released intermediates and products.

In the present work, we studied the impact of different oxidation technologies on the removal of maprotiline and their effect on the degradation pathways by monitoring the disappearance kinetics and the formation of transformation products by LC/HRMS; in-silico toxicity, estimations have been carried out on the TPs as well. For this purpose, different AOPs were considered: (i) semiconductors photocatalysis: Iron-doped zinc oxide

(Fe-ZnO), cerium doped zinc oxide (Ce-ZnO) and TiO₂; (ii) heterogeneous photo-Fenton: magnetite coated with humic acid (Fe₃O₄/HA) for the activation of H₂O₂ and S₂O₈²⁻).

2. Results

2.1. Maprotiline Photoinduced Degradation

For each advanced oxidation technology, maprotiline removal was followed by LC/HRMS in ESI positive ion mode, monitoring the protonated molecule at m/z 278.1911. As reported in Figure 1, no significant maprotiline removal was observed using direct photolysis under UVA irradiation, due to its low radiation absorption above 280 nm [37]. These results are in agreement with the long half-life time previously observed in river water under irradiation [36,38]. The experiments performed by means of different oxidation approaches showed that all the materials were able to remove maprotiline completely in less than 40 min under irradiation. The semiconductor photocatalysts proved to be the most efficient, removing the drug with kinetics faster than those of the photo-Fenton systems.

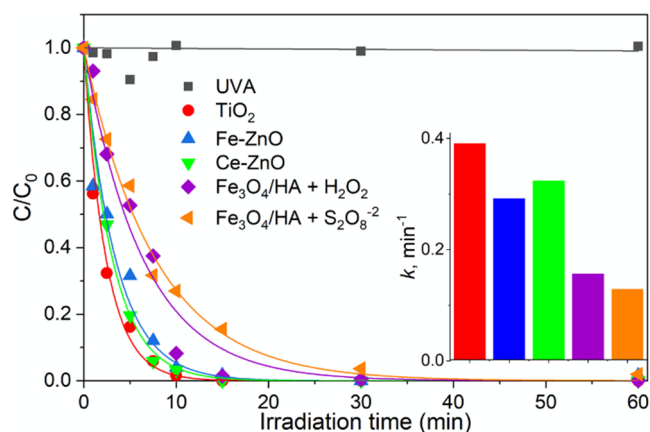


Figure 1. Maprotiline removal in the presence of different oxidation processes under UVA irradiation: photocatalysis using TiO₂, Fe-ZnO or Ce-ZnO, and heterogeneous photo-Fenton using Fe₃O₄/HA for the activation of H₂O₂ or S₂O₈²⁻. The inset compares the kinetic constant values.

The photo-Fenton-like processes, Fe₃O₄/HA exhibited slightly faster degradation kinetics in the presence of hydrogen peroxide comparing with the same system in the presence of persulfate. In all cases, a monoexponential decay was observed for maprotiline with the degradation time: $C/C_0 = \exp(-k \times t)$, where C_0 is the maprotiline initial concentration, C that at the reaction time t , and the pseudo-first-order kinetic constant k .

2.2. Maprotiline Transformation Products

Considering the aim of this study and how the different photocatalytic systems may affect the generation of TPs, samples were firstly analyzed by direct infusion in ESI positive mode, without any sample treatment, and the SPIX software was used to process HRMS data, to select statistically relevant ions from complex spectra. It should be noted that because of direct infusion analysis isomeric species are not distinguishable. Among the different degradation systems, SPIX allowed to ascertain maprotiline degradation and to extract a total of 10 m/z ratios appearing and disappearing over the photocatalytic degradation time, recognized as potential transformation products. The output data for the extracted ions and the kinetic models best fitting the ion abundance evolution over time are presented in Table S1 (Supplementary Materials). SPIX software allowed to ensure that potential singular species formed depending on the degradation system were not neglected due to operator-related subjectivity. For more information about SPIX functioning, please refer to Nicol et al. [39].

LC/HRMS experiments allowed identifying thirty-six species, interestingly all matching with those previously identified using the SPIX software in the form of several isomers,

as presented in Table 1. The species identified were named based on their $M+H^+$, e.g., 294-A corresponds to a isomer at m/z 294. In agreement with our previous studies [36], maprotiline degradation derives in several isomeric forms resulting from hydroxyl group addition(s) in several positions, namely mono- (m/z 294), di- (m/z 310), tri- (m/z 326) and tetra-hydroxylated (m/z 342) derivatives. From those, the corresponding dehydrogenated mono- (m/z 292), di- (m/z 308), and tri- hydroxylated (m/z 324) species were also identified. Species resulting from the ring-opening were also observed (m/z 284, 258, and 234).

Table 1. Summary of TPs resulting from maprotiline degradation under different AOPs.

Compound	[M+H] ⁺	Formula	Δ (ppm)	r.t. (min)	TiO ₂	Fe-ZnO	Ce-ZnO	Fe ₃ O ₄ /HA	
								H ₂ O ₂	S ₂ O ₈ ²⁻
Maprotiline	278.1911	C ₂₀ H ₂₄ N	−2.81	9.7					
294-A ^(a)	294.1858	C ₂₀ H ₂₄ NO	−1.98	7.3	+	+	+	+	-
294-B ^(a)				7.8	+	+	+	+	+
294-C ^(a)				8.0	+	+	+	+	+
294-D				8.3	+	+	+	+	+
294-E				8.9	+	+	+	+	+
310-A	310.1807	C ₂₀ H ₂₄ NO ₂	−2.00	6.9	+	+	+	+	-
310-B				7.2	+	+	+	+	-
310-C				7.4	+	+	+	+	-
310-D				8.0	+	+	+	+	+
310-E				8.2	+	+	+	+	-
310-F				8.5	+	+	+	+	+
326-A	326.1757	C ₂₀ H ₂₄ NO ₃	−2.13	6.1	+	+	+	+	+
326-B ^(a)				6.9	+	+	+	+	+
326-C ^(a)				7.6	+	+	+	+	+
342-A ^(a)	342.1707	C ₂₀ H ₂₄ NO ₄	−2.09	6.0	+	+	+	+	+
342-B ^(a)				6.4	+	+	+	+	+
342-C ^(a)				7.1	+	+	+	+	+
342-D				7.6	+	+	+	+	+
292-A	292.1701	C ₂₀ H ₂₂ NO	−2.06	6.9	+	+	+	+	-
292-B ^(a)				7.9	+	+	+	+	-
292-C ^(a)				8.5	+	+	+	+	-
292-D				8.6	+	+	+	+	-
292-E				9.1	+	+	+	+	+
308-A	308.1651	C ₂₀ H ₂₂ NO ₂	−1.96	6.4	+	+	+	+	-
308-B ^(a)				7.3	+	+	+	+	-
308-C ^(a)				7.7	+	+	+	+	+
324-A	324.1599	C ₂₀ H ₂₂ NO ₃	−1.70	5.8	+	+	+	+	+
324-B				6.4	-	-	-	-	+
324-C				7.0	-	-	-	-	+
324-D				7.9	-	-	-	-	+
284-A	284.1650	C ₁₈ H ₂₂ NO ₅	−1.75	6.7	+	+	+	+	+
284-B				7.3	+	+	+	+	+
284-C ^(a)				7.7	+	-	-	+	+
284-D				8.4	-	-	-	-	+
234 ^(a)	234.1492	C ₁₄ H ₂₀ NO ₂	−1.70	4.4	+	+	+	+	+
258	258.1493	C ₁₆ H ₂₀ NO ₂	−1.77	6.3	+	+	-	+	+

(+) detected; (-) not observed. ^(a) observed in wastewater treatment effluents by retrospective analysis [36].

The formed TPs evolution over time depending on the oxidation process are shown in Figure S1. This evidenced the formation of all TPs within a few minutes, exhibiting maximum intensity after 5 to 10 min of treatment and their complete disappearance after 30 min in presence of semiconductors photocatalysts and H₂O₂ activated by Fe₃O₄/HA. However, most of those species have a slower degradation profile when mediated by the persulfate, with maximum intensity observed at longer irradiation times even if also completely removed within 1 h, except the ion m/z 234 that is still present at the end of the experiment (see Figure S1). In a general way, most of the identified TPs are common

to all the oxidation processes with the exception of that using persulfate, which induces a specific behavior regarding some TPs. For instance, the persulfate system leads to the formation of four isomers with the formula $C_{20}H_{22}NO_3$ (MH^+ at m/z 324) against only one (324-A) for other AOPs. In the same way, the species 284-D and 308-C are also specifically formed with persulfate when other 284 and 308 isomers are common to all oxidation processes. Contrariwise, only one isomer (292-E) was observed for the ion at m/z 292 in the degradation promoted by the persulfate system, as shown in Table 1 and better evidenced in Figure S1. Similarly, only two out of the six species resulting from the dihydroxylation (MH^+ at m/z 310) were formed in the persulfate oxidation process. The collision induced dissociation data presented in Table S2 (Supplementary Materials) allowed making the correspondence between the TPs detected in the present study and those reported in a study devoted to UV-Vis maprotiline degradation, in which CID experiments led to propose TPs' chemical structures [36].

2.3. In Silico Bioassays

The in-silico toxicity was evaluated on maprotiline and on the previously elucidated TPs [36]; the results as summarized in Table 2. The mutagenicity prediction was performed using a consensus-based on four different models. Maprotiline was found to be non-mutagenic, in agreement with the available experimental data [40], as well as for all the TPs. The developmental/reproductive toxicity was estimated by the library model implementing a virtual library of toxicant compounds with endpoint indicators based on toxicant/non-toxicant [41]. Maprotiline, as well as 292-E, 284-B, 234, and 258 were estimated as non-toxicant, while, the remaining TPs were predicted as a toxicant, with the potential to impact the developmental/reproductive abilities.

Table 2. Toxicity values estimated by the VEGA software for maprotiline and the main degradation products.

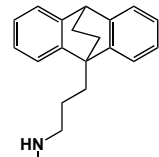
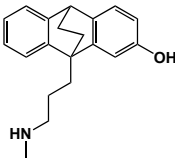
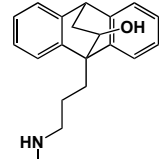
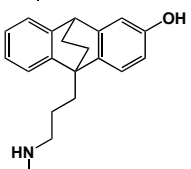
Compound	Mutagenicity (AMES test)	Developmental/Reproductive Toxicity	F. Minnow LC50 (96 h) ($mg L^{-1}$)	D. Magna LC50 (48 h) ($mg L^{-1}$)	Fish Acute LC50 (48 h) ($mg L^{-1}$)
MPT 	Negative	Non-toxicant	2.61	0.08	1.29
294-A 	Negative	Toxicant	3.13	0.20	1.68
294-B 	Negative	Toxicant	7.15	0.31	2.43
294-C 	Negative	Toxicant	3.10	0.21	1.61

Table 2. Cont.

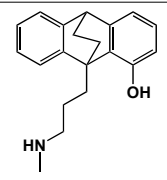
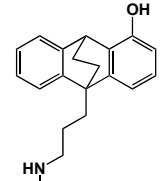
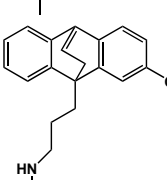
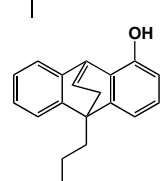
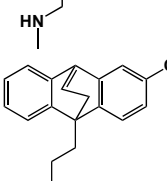
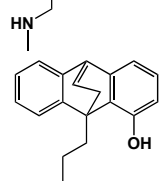
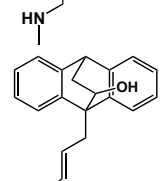
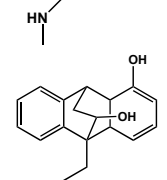
Compound	Mutagenicity (AMES test)	Developmental/Reproductive Toxicity	F. Minnow LC50 (96 h) (mg L ⁻¹)	D. Magna LC50 (48 h) (mg L ⁻¹)	Fish Acute LC50 (48 h) (mg L ⁻¹)	
294-D		Negative	Toxicant	2.00	0.22	1.58
294-E		Negative	Toxicant	2.52	0.23	1.57
292-A		Negative	Toxicant	3.21	0.16	2.06
292-B		Negative	Toxicant	2.59	0.18	2.17
292-C		Negative	Toxicant	3.19	0.16	1.59
292-D		Negative	Toxicant	2.06	0.18	1.86
292-E		Negative	Non-toxicant	8.82	0.28	3.39
310-A		Negative	Toxicant	8.02	5.25	3.85

Table 2. Cont.

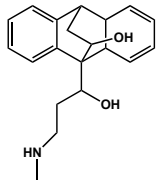
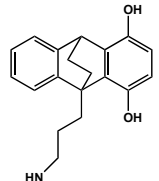
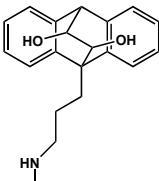
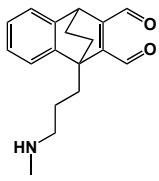
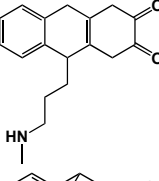
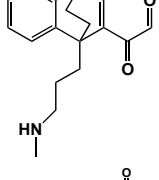
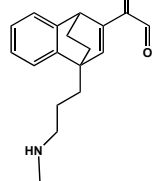
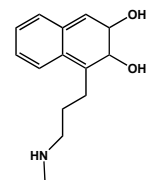
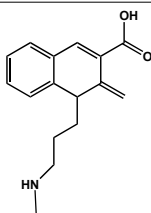
Compound	Mutagenicity (AMES test)	Developmental/Reproductive Toxicity	F. Minnow LC50 (96 h) (mg L ⁻¹)	D. Magna LC50 (48 h) (mg L ⁻¹)	Fish Acute LC50 (48 h) (mg L ⁻¹)	
310-B		Negative	Toxicant	26.12	6.29	5.70
310-E		Negative	Toxicant	2.37	4.44	3.14
310-F		Negative	Toxicant	13.88	5.47	5.54
284-A		Negative	Toxicant	0.47	0.14	5.58
284-B		Negative	Non-toxicant	8.81	0.26	8.00
284-C		Negative	Toxicant	1.92	0.12	5.11
284-D		Negative	Toxicant	2.09	0.12	4.35
234		Negative	Non-toxicant	48.19	36.35	5.89

Table 2. Cont.

Compound	Mutagenicity (AMES test)	Developmental/Reproductive Toxicity	F. Minnow LC50 (96 h) (mg L ⁻¹)	D. Magna LC50 (48 h) (mg L ⁻¹)	Fish Acute LC50 (48 h) (mg L ⁻¹)
258 	Negative	Non-Toxicant	4.97	0.73	5.89

Fathead minnow LC50 (96 h) test represents the concentration that results in the mortality of half of the fish population (*Pimephales promelas*) in 96 h. The software-based on EPA model estimates similar toxicity for the drug and TPs resulting from the drug mono-hydroxylation and the corresponding dehydrogenated species, except for the species resulting from the addition of a hydroxyl group onto the ethylene bridge (294-B and 292-E), which were estimated 3/4 times less toxicant. Among the di-hydroxylated species, those resulting from addition onto the ethylene bridge were estimated as significantly less toxic, comparing with the one resulting from hydroxylation onto the phenyl ring (310-E). Among all TPs, only the specie 284-A was estimated as significantly toxicant, with an LC50 value much lower (0.47 mg L⁻¹) than that of maprotiline (2.61 mg L⁻¹).

The predicted lethal concentration dose for half of the population of *Daphnia Magna* within 48 h (EPA model) is lower for maprotiline (0.08 mg L⁻¹) than for all the tested TPs (ranging from 0.12 to 36.35 mg L⁻¹). Even if less toxic, the species with *m/z* 294, 292, 284, and 258 were considered as toxicants while those resulting from dihydroxylation were estimated as slightly toxic. Likewise, the species with *m/z* 234 was estimated as having a significantly lower toxic effect. A similar trend was estimated for fish acute lethal dose concentration where the TPs are predicted as less toxicant (LC50 between 1.58 and 8.00 mg L⁻¹) than the parent compound (LC50 estimated at 1.29 mg L⁻¹). As observed before, TPS resulting from the ring-opening and addition of multiple hydroxyl groups were estimated as less toxicant, i.e., *m/z* 310 isomers, particularly those resulting from the bridge hydroxylation.

3. Discussion

As evidenced in Figure 1, semiconductor catalysts proved to be the most efficient for maprotiline removal. No significant difference was observed among the investigated semiconductors, with a slightly faster removal efficiency observed for TiO₂. These results contrast with the substantially higher efficiency of Ce-ZnO materials compared to TiO₂ reported for the degradation of several x-ray contrast agents [42]. Additionally, it is worth noting that no considerable differences in the TPs evolution over time were observed due to the semiconductor applied, as evidenced in Figure S1 (Supplementary Materials). This can be justified by the fact that all those photocatalysts have a similar mechanism for the generation of reactive species. The photoexcitation mechanisms of TiO₂ and ZnO based photocatalysts are characterized by the formation of HO• radicals, that can then react with organic pollutants [43].

As shown in Figure 1, the heterogeneous photo-Fenton catalyst in the presence of persulfate showed a slightly lower efficiency towards maprotiline removal than hydrogen peroxide. In previous studies, Fe₃O₄/HA demonstrated high efficiency for water pollutants removal through the catalytic activation of hydrogen peroxide and persulfate [29]. By the addition of isopropanol, a selective HO• scavenger, to the hydrogen peroxide system the strong inhibition in the degradation rate pointed out the HO• radical as the main responsible during the oxidation process. When in the presence of persulfate, the addition of radical scavengers allowed to confirm the SO₄•⁻ as responsible for the degradation process.

The lower reduction potential of persulfate radical ($E_{\text{SO}_4^{\bullet-}/\text{SO}_4^{2-}}^{\circ} = 2.4 \text{ V}$) [44,45] to react with organic pollutants compared to that hydroxyl radical ($E_{\text{HO}^{\bullet}+\text{H}^+/\text{H}_2\text{O}}^{\circ} = 2.74 \text{ V}$), [45] could be the explanation for the slower degradation rate. Moreover, the reaction of HO^{\bullet} with organic pollutants mainly involves: (i) Hydrogen atom abstraction, reaction possible for the oxidation of saturated hydrocarbons and (ii) radical addition to double bonds or aromatic rings, usually reacting very fast, sometimes controlled by the diffusion. For sulfate radical, one-electron-reactions are favored—one electron is transferred from the pollutant to $\text{SO}_4^{\bullet-}$ generating the molecular radical and sulfate ion (Equation (1), followed by pollutants hydroxylation with water or OH^- [46,47]:



The electron transfer reaction is easier with pollutants that have electron-donating groups and less likely for those with electron-withdrawing, such as aromatic compounds [48]. This point, together with the H abstraction reaction and the addition reaction may explain the faster maprotiline degradation for HO^{\bullet} mediated processes in comparison with those using $\text{SO}_4^{\bullet-}$.

Yang et al. reported a slower ibuprofen degradation kinetics using $\text{SO}_4^{\bullet-}$ instead of HO^{\bullet} ; a theoretical study attributed this effect to the steric hindrance of $\text{SO}_4^{\bullet-}$, for which the reaction process presents energy barriers significantly higher than that involving HO^{\bullet} [49]. These intrinsic differences between $\text{SO}_4^{\bullet-}$ and HO^{\bullet} could also explain the differences in TPs formation. In the case of the persulfate system, the formation of only one m/z 292 isomer out of five, issued from H_2 elimination from m/z 294 photoproducts, could be justified by the steric hindrance of $\text{SO}_4^{\bullet-}$. The fact that only the specie 292-E, which specifically results from H_2 elimination from the alkyl chain is in good agreement with this hypothesis.

As a consequence of the lower efficiency of the persulfate system, one could expect fewer TPs resulting from multi-hydroxylation but this was not the case. In fact, the $\text{SO}_4^{\bullet-}$ seems to promote the formation of more multi-hydroxylated isomers at m/z 324 rather than the HO^{\bullet} mediated processes.

From the in-silico toxicity predictions shown in Table 2 and better evidenced by the frequency as a function of Log (LC_{50}) presented in Figure 2, all the TPs were estimated with similar or lower toxicant properties of the antidepressant drug for both *Daphnia magna* and *Fish acute*. In the case of *Fathead minnow*, the species 284-A, which carries two aldehyde functions, was predicted as significantly more toxicant than all other TPs. Based on the predicted LC_{50} values, TPs can be dispatched into the 4 categories of concern defined by the EPA (Environmental Protection Agency): category 1 ($\text{LC}_{50} < 0.1 \text{ mg L}^{-1}$), category 2 ($0.1 < \text{LC}_{50} < 1 \text{ mg L}^{-1}$), category 3 ($1 < \text{LC}_{50} < 10 \text{ mg L}^{-1}$) and category 4 ($10 < \text{LC}_{50} < 100 \text{ mg L}^{-1}$), [50]. The frequency distribution of TPs, shown in Figure 2, made it clear that potentially higher toxicant properties of several intermediates comparing with the parent compound. These results are in agreement with those previously observed by the *vibrio fischeri* toxicity test for the mixture obtained during the maprotiline degradation in the presence of TiO_2 photocatalyst [36]. It was reported an increase in the bioluminescence inhibition of the target organism during the first degradation stage attributed to the slightly more toxic TPs.

A correlation was found between the number of hydroxyl groups and the predicted toxicity, e.g., dehydroxylated isomers of TPs with m/z at 310 are estimated with higher lethal dose concentrations than the mono-hydroxylated species (m/z 294). Lower toxicant properties were estimated for TPs resulting from hydroxylation onto the bridge rather than onto aromatic rings, e.g., 294-B seems less toxic than the others m/z 294 isomers. As evidenced in Table 2, this species has been previously identified by retrospective analysis of wastewater treatment plant effluents resulting from current remediation processes [36]. Additionally, the species resulting from ring-opening (m/z 284, 234, and 258), observed with higher persistence for degradation mediated by $\text{SO}_4^{\bullet-}$, showed significantly lower

toxicant effect than maprotiline for all the different endpoint indicators, except for 284-A. It should be pointed out that even if the m/z 234 was still present at the end of the irradiation time, considering its lower toxicant properties, no significant harmful impacts can be anticipated by using persulfate rather than other oxidative processes. Notably, this species was also reported in the wastewater treatment plant effluents (Table 2).

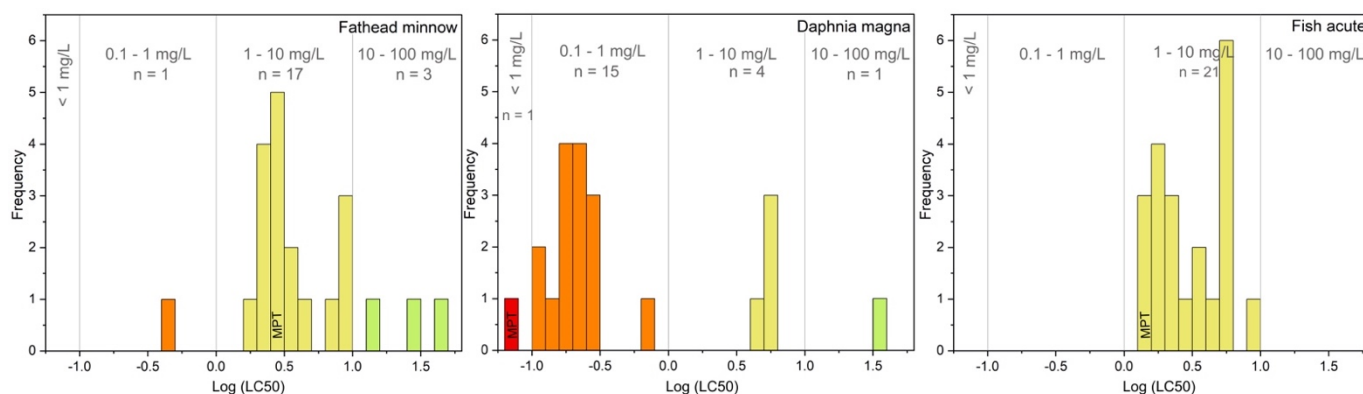


Figure 2. Distribution of TPs estimated Log (LC₅₀) thresholds (mg L⁻¹), based on EPA acute aquatic concerning categories.

Even if the estimated lethal dose toxicity for maprotiline and respective TPs was in the mg L⁻¹ concentration range—considerably higher than what is expected to be released in the environment—studies with environmentally relevant concentrations are strongly needed to understand the potentially harmful effects of those substances on aquatic biota. For example, fluoxetine (another antidepressant drug) was estimated with acute toxicity LC₅₀ = 5.91 mg L⁻¹ on *Daphnia magna* [51]. However, it has been reported to alter the swimming behavior and camouflage efficiency of invertebrates even at very low concentrations (1–100 ng L⁻¹) [52,53]. Additionally, Weinberger et al., at the same concentration range observed a significant impact on mating, defensive, aggressive and isolation behaviors of fish fathead minnow [54]. These issues raise the importance of the wastewater treatment plants to efficiently removing the unregulated contaminants of emerging concern but also their degradation products. Also, it is of high interest to extend the studies on mixture effects as different contaminants and TPs can have a synergistic effect in terms of toxicity.

4. Materials and Methods

4.1. Chemicals

Maprotiline hydrochloride (CAS: 10347-81-6), was purchased from Sigma-Aldrich (Milan, Italy). All precursors and reagents used for the synthesis of materials and subsequent analyzes were purchased from Sigma-Aldrich (Milan, Italy) too. FeCl₃·6H₂O and FeSO₄·7H₂O were purchased from Carlo Erba Reagents (Milan, Italy); humic acid sodium salts (technical, 50–60% as HA) from Aldrich-Chemie. Acetonitrile and formic acid were purchased from Sigma Aldrich (Saint-Quentin-Fallavier, France). TiO₂ (Evonik P25, Frankfurt, Germany), to avoid possible interference from ions adsorbed on the photocatalyst, was irradiated and washed with distilled water, until there were no detectable signals due to chloride, sulfate, and sodium ions.

4.2. Preparation of Catalysts

4.2.1. Fe(0.5%)ZnO and Ce(1%)ZnO

Zinc oxide materials doped with iron and cerium were prepared by the hydrothermal method previously described [25,42]. In detail, the doping agent, FeCl₃ or CeCl₃·7H₂O, was added in the desired molar concentration to a 1 M solution of Zn(NO₃)₂·6H₂O (20 mL) under continuous stirring. A solution of NaOH 4 M was added dropwise until reaching a pH value of 10–11. The solution was transferred into a 100 mL Teflon-lined autoclave,

completed with water up to 50 mL, and kept at 175 °C for 15 h. The resulting precipitate was washed with water and recovered by centrifugation (6000 rpm for 10 min), repeating the procedure 2 times. After drying at 70 °C overnight, the powders were homogenized using a mortar and pestle.

4.2.2. Fe₃O₄/HA

Humic coated magnetite particles were prepared by co-precipitation under nitrogen atmosphere as previously reported [28]. Briefly, 35 mL of a solution of FeCl₃·6H₂O 0.68 M and FeSO₄·7H₂O 0.43 M (molar ratio Fe(III)/Fe(II) = 1.5) were added to 65 mL of deoxygenated water at 90 °C, under vigorous mechanic stirring and N₂ continuous flow. 10 mL of ammonium hydroxide (25%) and 50 mL of a 0.5 wt. % HA solution were added rapidly and sequentially. The reaction was kept for 30 min at 90 °C, then cooled down to room temperature under continuous nitrogen flow. The obtained magnetite particles (Fe₃O₄/0.5 HA) were centrifuged and washed four times with 40 mL of water; they were then dried in a tube furnace under nitrogen flow at 80 °C for 15 h and manually crumbled.

4.3. Methods

4.3.1. Photodegradation Experiments under UVA Irradiation

The photocatalytic experiments were carried out in Pyrex glass cells kept under magnetic stirring and containing 5 mL of maprotiline (5 mg L⁻¹) and catalyst (100 mg L⁻¹) solution at room temperature. Samples were irradiated for different times up to 60 min using a Cleo 6x15 W TL-D Actinic BL (290–400 nm range, 90 ± 2 W m⁻²) lamp (Philips, Milan, Italy) with maximum emission at 365 nm, measured with a CO.FO.ME.GRA (Milan, Italy) power meter.

The photo-Fenton-like experiments were performed in the previously optimized conditions [28]. In detail, the hydrogen peroxide (1.0 mM) was added to the suspension of Fe₃O₄/HA (100 mg L⁻¹) adjusted at pH 3, while sodium persulfate (1.0 mM) was added to the suspension at pH 6. The pH was adjusted using H₂SO₄. After irradiation, 0.33 mL of methanol was added to the 5 mL of the suspension to quench the thermal Fenton reaction. All the samples were filtered using a 0.45 µm hydrophilic PTFE filter (Minisart® SRP15 Syringe Filter 17574, Sartorius, Göttingen, Germany). An equilibration time of 30 min was always applied to follow possible adsorption and in-dark degradation.

4.3.2. Analysis

LC-MS and LC-MSⁿ measurements were performed on an Acquity HPLC system (Water Technologies, Guyancourt, France) coupled with a Bruker SolarixXR FT-ICR 9.4 T MS instrument (Bruker Daltonics, Bremen, Germany). An Agilent Pursuit XRs^{ULTRA} C18 (length 50 mm, diameter 2 mm, particle size 2.8 µm) column was used with an Agilent HPLC MetaGuard (Pursuit XRs C18, 3 µm, 2 mm) guard column (Agilent Technologies, Les Ulis, France). The flow was set to 0.2 mL/min, the total run time was 22 min with an acquisition time of 15 min. Gradient flow was used with solvent A being water with 0.1% formic acid and solvent B being acetonitrile with 0.1% formic acid. The LC method consisted of holding 95% of solvent A and 5% of solvent B for 3 min, after which a gradient of 9 min was applied until the ratio of the two solvents reached 50–50%. The ratio of solvent A was promptly decreased to 5% and kept at this ratio until 17.1 min total run time, after it was reset to the initial 95%. After every measurement, 5 min were left for equilibration and washing at this latter solvent ratio.

The injection volume was 2 µL and 10 µL for LC-MS and LC-MSⁿ experiments, respectively. The sample manager was kept at 4 °C for better preservation. Each sample was prepared for the analysis by adding 10% volume of a mixture of acetonitrile/formic acid (0.1%). Electrospray ionization was used as the ion source in positive mode with a sample flow of 0.2 mL/min. The capillary voltage was 4000 V and the spray shield was set at -500 V. Nitrogen was used as nebulizer gas (1 bar) and drying gas (8 L/min, 250 °C). The detection range was 57.7–1000 m/z, in broadband mode, with a data acquisition size

of 4 Mpts and a data reduction of noise of 97%. For MS² experiments, isolation was carried out with a 1 m/z window and collision-induced dissociation experiments were performed with energies of 5, 10, 15, and 20 V. Preliminary in-cell experiments were performed to assess the optimal parameters (isolation window, quadrupole voltage, and collision energy) for the MS³ experiments. Measurements were also completed on the FT-ICR using direct infusion. In this case, the flow rate was 120 µL/h, with an acquisition of 4 Mpts, using the same m/z range as for LC-MS measurements. The ion accumulation time was 0.1 s and 100 scans were recorded for each spectrum. The Bruker DataAnalysis software was used for data processing.

Dealing with HRMS complex data sets is generally tricky, mainly because of (i) the experimental errors and uncertainties induced during sample preparation and analysis, (ii) the intrinsic variability of samples, (iii) the operator's subjectivity when facing mass spectra, including hundreds or thousands of ions. That is why the SPIX software has been recently developed, which is capable of analyzing a set of mass spectra at once, taking into account the intrinsic variability of the samples and that induced by HRMS measurements [39]. One feature of SPIX is to extract from a set of complex spectra all the ions that undergo significant change over time during a given process; it carries out statistical calculations aiming at fitting the evolution of an ion abundance to one of the exponential kinetic models contained in a library or a polynomial model which fits best the evolution of the ion. This permits to reveal the decrease of a parent compound, as well as the appearance and eventual disappearance of intermediates and products. The software attributes an R² value for the goodness of the fitting, as well as a statistical significance value (*p*-value).

In the present study, 5 measurements were performed over time, for each catalytic system; SPIX was run with the mass spectra data set of each system, in order to monitor maprotiline photodegradation and reveal intermediates and products that are statistically relevant considering experimental uncertainties. Experiments were performed using positive direct infusion MS, with minimal a priori sample preparation.

4.3.3. In-Silico Bioassays

Preliminary ecotoxicity assessments were performed using the VEGA QSAR software (website: <https://www.vegahub.eu/>, version 1.1.5 beta 22, accessed on 25 November 2020) developed by Politecnico di Milano, Italy [55]. VEGA is based on quantitative structure-activity relationship model platforms, which provide detailed information and analysis to support a toxicity prediction from different models. The models on VEGA platform were built following the OECD principles for acceptance of QSAR models for regulatory use.

The endpoint for each individual model is assessed based on a scale of reliability. Mutagenicity (AMES test) was predicted by CONSENSUS model supported by four different models (CAESAR—version 2.1.13; SarPy—version 1.0.7; ISS—version 1.0.2 and KNN—version 1.0.0). Developmental/Reproductive Toxicity models were estimated by the library (PG) (version 1.1.0). The tests for *Fathead minnow* LC₅₀ (96 h) and *Daphnia magna* LC₅₀ (48 h) were predicted by EPA model (version 1.0.7) based on T.E.S.T. software developed by US EPA [52]. The quantitative model for Fish acute toxicity (LC₅₀) was performed by the toxicity IRFMN model (version 1.0.0).

5. Conclusions

Semiconductor oxides proved to be more efficient for maprotiline removal than photo-Fenton-like processes. The degradation trends followed the order: TiO₂ > Ce-ZnO > Fe-ZnO > Fe₃O₄/HA + H₂O₂ > Fe₃O₄/HA + S₂O₄²⁻. The degradation process mediated by SO₄^{•-} led to slower degradation and slower intermediates disappearance in comparison with OH[•] mediated processes. The in-house developed SPIX software tackled the subjectivity, finding those with statistically significant change throughout the experimental time. A total of thirty-six TPs were identified using LC-HRMS; they result from drug multi-hydroxylation, oxidation, and ring-opening. The application of different AOPs demonstrated to have

an impact on the formation of diverse TPs attributed mainly to the oxidation species involved. In-silico bioassays estimated similar or lower toxicity for the majority of the investigated TPs compared to the parent compound, finding no correlation between the applied oxidation process and the toxicity.

Supplementary Materials: The following are available online at <https://www.mdpi.com/2073-4344/11/2/240/s1>, Figure S1: Evolution over time of maprotiline degradation products formed in the presence of different catalysts under UVA irradiation., Table S1: Summary of SPIX software output data from maprotiline and potential TPs, Table S2: Summary of [M+H]⁺ and their main fragments from CDI experiments, together with the empirical formula.

Author Contributions: Conceptualization, P.C., N.P.F.G. and Z.V.; software, Z.V.; validation, Z.V., E.N. and S.B.; investigation, N.P.F.G. and Z.V.; data curation, N.P.F.G. and Z.V.; writing—original draft preparation, N.P.F.G.; writing—review and editing, N.P.F.G., P.C., Z.V. and S.B.; supervision, P.C. and S.B.; funding acquisition, P.C. and S.B. All authors have read and agreed to the published version of the manuscript.

Funding: This work is part of a project that has received funding from the European Union’s Horizon 2020 research and innovation program under the Marie Skłodowska-Curie grant agreement No 765860. Authors also acknowledge the financial support for experiments provided by the Region Council of Auvergne, from the “Fédération des Recherches en Environnement” through the CPER “Environment” founded by the Region Auvergne, the French government, FEDER from the European Community and from CAP 20e25 I-site project. Financial support from the National FT-ICR network (FR 3624 CNRS) for conducting the research is gratefully acknowledged.

Data Availability Statement: Not applicable.

Conflicts of Interest: The authors declare no conflict of interest.

References

1. Taheran, M.; Naghdi, M.; Brar, S.K.; Verma, M.; Surampalli, R.Y. Emerging contaminants: Here today, there tomorrow! *Environ. Nanotechnol. Monit. Manag.* **2018**, *10*, 122–126. [[CrossRef](#)]
2. Petrie, B.; Barden, R.; Kasprzyk-Hordern, B. A review on emerging contaminants in wastewaters and the environment: Current knowledge, understudied areas and recommendations for future monitoring. *Water Res.* **2014**, *72*, 3–27. [[CrossRef](#)] [[PubMed](#)]
3. Starling, M.C.V.M.; Amorim, C.C.; Leão, M.M.D. Occurrence, control and fate of contaminants of emerging concern in environmental compartments in Brazil. *J. Hazard. Mater.* **2019**, *372*, 17–36. [[CrossRef](#)]
4. Ebele, A.J.; Abdallah, M.E.; Harrad, S. Pharmaceuticals and personal care products (PPCPs) in the freshwater aquatic environment. *Emerg. Contam.* **2017**, *3*, 1–16. [[CrossRef](#)]
5. Das, S.; Ray, N.M.; Wan, J.; Khan, A.; Chakraborty, T.; Ray, M.B. Micropollutants in Wastewater: Fate and Removal Processes. In *Physico-Chemical Wastewater Treatment and Resource Recovery*; In Tech: Rijeka, Croatia, 2017; pp. 75–107.
6. Lindberg, R.H.; Östman, M.; Olofsson, U.; Grabic, R.; Fick, J. Occurrence and behaviour of 105 active pharmaceutical ingredients in sewage waters of a municipal sewer collection system. *Water Res.* **2014**, *58*, 221–229. [[CrossRef](#)] [[PubMed](#)]
7. Nguyen, T.T.; Westerhoff, P.K. Drinking water vulnerability in less-populated communities in Texas to wastewater-derived contaminants. *NPJ Clean Water* **2019**, *2*, 1–9. [[CrossRef](#)]
8. Abbing-Karahagopian, V.; Huerta, C.; Souverein, P.C.; De Abajo, F.; Leufkens, H.G.M.; Slattery, J.; Alvarez, Y.; Miret, M.; Gil, M.; Oliva, B.; et al. Antidepressant prescribing in five European countries: Application of common definitions to assess the prevalence, clinical observations, and methodological implications. *Eur. J. Clin. Pharmacol.* **2014**, *70*, 849–857. [[CrossRef](#)] [[PubMed](#)]
9. Bachmann, C.J.; Aagaard, L.; Burcu, M.; Glaeske, G.; Kalverdijk, L.J.; Petersen, I.; Schuiling-Veninga, C.C.; Wijlaars, L.; Zito, J.M.; Hoffmann, F. Trends and patterns of antidepressant use in children and adolescents from five western countries, 2005–2012. *Eur. Neuropsychopharmacol.* **2016**, *26*, 411–419. [[CrossRef](#)]
10. Ford, A.T.; Herrera, H. ‘Prescribing’ psychotropic medication to our rivers and estuaries. *BJ Psych. Bull.* **2019**, *43*, 147–150. [[CrossRef](#)]
11. Vandermeersch, G.; Lourenço, H.M.; Alvarez-Muñoz, D.; Cunha, S.; Diogène, J.; Cano-Sancho, G.; Sloth, J.J.; Kwadijk, C.; Barcelo, D.; Allegaert, W.; et al. Environmental contaminants of emerging concern in seafood—European database on contaminant levels. *Environ. Res.* **2015**, *143*, 29–45. [[CrossRef](#)]
12. Sehonova, P.; Svobodova, Z.; Dolezelova, P.; Vosmerova, P.; Faggio, C. Effects of waterborne antidepressants on non-target animals living in the aquatic environment: A review. *Sci. Total Environ.* **2018**, *631–632*, 789–794. [[CrossRef](#)] [[PubMed](#)]
13. Martin, J.M.; Saaristo, M.; Tan, H.; Bertram, M.G.; Nagarajan-Radha, V.; Dowling, D.K.; Wong, B.B.M. Field-realistic antidepressant exposure disrupts group foraging dynamics in mosquitofish. *Biol. Lett.* **2019**, *15*, 20190615. [[CrossRef](#)]

14. Loos, R.; Carvalho, R.; António, D.C.; Comero, S.; Locoro, G.; Tavazzi, S.; Paracchini, B.; Ghiani, M.; Lettieri, T.; Blaha, L.; et al. EU-wide monitoring survey on emerging polar organic contaminants in wastewater treatment plant effluents. *Water Res.* **2013**, *47*, 6475–6487. [[CrossRef](#)] [[PubMed](#)]
15. Baresel, C.; Cousins, A.P.; Ek, M.; Ejhed, H.; Allard, A.-S.; Magnér, J.; Westling, K.; Fortkamp, U.; Wahlberg, C.; Hörsing, M.; et al. Pharmaceutical residues and other emerging substances in the effluent of sewage treatment plants. Review on concentrations, quantification, behaviour, and removal options. *Swed. Environ. Res. Inst. Rep. B* **2015**, 2226.
16. UNESCO; HELCOM. *Pharmaceuticals in the Aquatic Environment of the Baltic Sea Region—A Status Report. UNESCO Emerging Pollutants in Water Series—No. 1*; Minna, P.S.Z., Ed.; UNESCO Publishing: Paris, France, 2017; ISBN 9789231002137.
17. Deng, Y.; Zhao, R. Advanced Oxidation Processes (AOPs) in Wastewater Treatment. *Curr. Pollut. Rep.* **2015**, *1*, 167–176. [[CrossRef](#)]
18. Zhang, M.; Dong, H.; Zhao, L.; Wang, D.; Meng, D. A review on Fenton process for organic wastewater treatment based on optimization perspective. *Sci. Total Environ.* **2019**, *670*, 110–121. [[CrossRef](#)] [[PubMed](#)]
19. Bokare, A.D.; Choi, W. Review of iron-free Fenton-like systems for activating H₂O₂ in advanced oxidation processes. *J. Hazard. Mater.* **2014**, *275*, 121–135. [[CrossRef](#)]
20. Demarchis, L.; Minella, M.; Nisticò, R.; Maurino, V.; Minero, C.; Vione, D. Photo-Fenton reaction in the presence of morphologically controlled hematite as iron source. *J. Photochem. Photobiol. A Chem.* **2015**, *307–308*, 99–107. [[CrossRef](#)]
21. Nosaka, Y.; Nosaka, A. Understanding Hydroxyl Radical (•OH) Generation Processes in Photocatalysis. *ACS Energy Lett.* **2016**, *1*, 356–359. [[CrossRef](#)]
22. Nosaka, Y.; Nosaka, A.Y. Generation and Detection of Reactive Oxygen Species in Photocatalysis. *Chem. Rev.* **2017**, *117*, 11302–11336. [[CrossRef](#)] [[PubMed](#)]
23. Barakat, M.A.; Kumar, R. *Photocatalytic Activity Enhancement of Titanium Dioxide Nanoparticles*; Springer International Publishing: Cham, Switzerland, 2016; ISBN 978-3-319-24269-9.
24. Hu, K.; Li, R.; Ye, C.; Wang, A.; Wei, W.; Hu, D.; Qiu, R.; Yan, K. Facile synthesis of Z-scheme composite of TiO₂ nanorod/g-C₃N₄ nanosheet efficient for photocatalytic degradation of ciprofloxacin. *J. Clean Prod.* **2020**, *253*, 120055. [[CrossRef](#)]
25. Kumar, S.G.; Rao, K.S.R.K. Zinc oxide based photocatalysis: Tailoring surface-bulk structure and related interfacial charge carrier dynamics for better environmental applications. *RSC Adv.* **2015**, *5*, 3306–3351. [[CrossRef](#)]
26. Paganini, M.C.; Giorgini, A.; Gonçalves, N.P.F.; Gionco, C.; Bianco Prevot, A.; Calza, P. New insight into zinc oxide doped with iron and its exploitation to pollutants abatement. *Catal. Today* **2019**, *328*, 230–234. [[CrossRef](#)]
27. Gionco, C.; Paganini, M.C.; Giamello, E.; Burgess, R.; Di Valentin, C.; Pacchioni, G. Cerium-doped zirconium dioxide, a visible-light-sensitive photoactive material of third generation. *J. Phys. Chem. Lett.* **2014**, *5*, 447–451. [[CrossRef](#)]
28. Gonçalves, N.P.F.; Minella, M.; Fabbrì, D.; Calza, P.; Malitesta, C.; Mazzotta, E.; Bianco, A. Humic acid coated magnetic particles as highly efficient heterogeneous photo-Fenton materials for wastewater treatments. *Chem. Eng. J.* **2020**, *390*, 124619. [[CrossRef](#)]
29. Gonçalves, N.P.F.; Minella, M.; Mailhot, G.; Brigante, M.; Bianco Prevot, A. Photo-activation of persulfate and hydrogen peroxide by humic acid coated magnetic particles for Bisphenol A degradation. *Catal. Today* **2019**, in press.
30. Cory, W.C.; Welch, A.M.; Ramirez, J.N.; Rein, L.C. Naproxen and Its Phototransformation Products: Persistence and Ecotoxicity to Toad Tadpoles (*Anaxyrus terrestris*), Individually and in Mixtures. *Environ. Toxicol. Chem.* **2019**, *38*, 2008–2019. [[CrossRef](#)] [[PubMed](#)]
31. Ellepola, N.; Ogas, T.; Turner, D.N.; Gurung, R.; Maldonado-Torres, S.; Tello-Aburto, R.; Patidar, P.L.; Rogelj, S.; Piyasena, M.E.; Rubasinghe, G. A toxicological study on photo-degradation products of environmental ibuprofen: Ecological and human health implications. *Ecotoxicol. Environ. Saf.* **2020**, *188*, 109892. [[CrossRef](#)] [[PubMed](#)]
32. Boxall, A.B.A.; Sinclair, C.J.; Fenner, K.; Kolpin, D.; Maund, S.J. When Synthetic Chemicals Degrade in the Environment. *Environ. Sci. Technol.* **2004**, *70*, 368–375. [[CrossRef](#)]
33. Salimi, M.; Esrafil, A.; Gholami, M.; Jonidi, J.A.; Rezaei, K.R.; Farzadkia, M.; Kermani, M.; Sobhi, H.R. Contaminants of emerging concern: A review of new approach in AOP technologies. *Environ. Monit. Assess.* **2017**, *189*, 414–436. [[CrossRef](#)] [[PubMed](#)]
34. Chong, M.N.; Jin, B.; Chow, C.W.K.; Saint, C. Recent developments in photocatalytic water treatment technology: A review. *Water Res.* **2010**, *44*, 2997–3027. [[CrossRef](#)]
35. Xu, X.; Pliego, G.; Zazo, J.A.; Liu, S.; Casas, J.A.; Rodriguez, J.J. Two-step persulfate and Fenton oxidation of naphthenic acids in water. *J. Chem. Technol. Biotechnol.* **2018**, *93*, 2262–2270. [[CrossRef](#)]
36. Gonçalves, N.P.F.; Varga, Z.; Bouchonnet, S.; Dulio, V.; Alygizakis, N.; Bello, F.D.; Medana, C.; Calza, P. Study of the photoinduced transformations of maprotiline in river water using liquid chromatography high-resolution mass spectrometry. *Sci. Total Environ.* **2020**, *755*, 143556. [[CrossRef](#)]
37. Suh, S.K.; Smith, J.B. Maprotiline Hydrochloride. *Anal. Profiles Drug Subst. Excip.* **1986**, *15*, 393–426.
38. Blum, K.M.; Norström, S.H.; Golovko, O.; Grabic, R.; Järhult, J.D.; Koba, O.; Söderström Lindström, H. Removal of 30 active pharmaceutical ingredients in surface water under long-term artificial UV irradiation. *Chemosphere* **2017**, *176*, 175–182. [[CrossRef](#)] [[PubMed](#)]
39. Nicol, E.; Xu, Y.; Varga, Z.; Kinani, S.; Bouchonnet, S.; Lavielle, M. SPIX: A new software package to reveal chemical reactions at trace amounts in very complex mixtures from high-resolution mass spectra data sets. *Rapid Commun. Mass Spectrom.* **2020**, *35*, e9015.
40. Wells, B.G.; Pharm, D.; Gelenberg, A.J. Adverse Effects, and Efficacy of the Antidepressant Maprotiline Hydrochloride. *Pharmacother. J. Hum. Pharmacol. Drug Ther.* **1981**, *1*, 121–138. [[CrossRef](#)]

41. Wu, S.; Fisher, J.; Naciff, J.; Laufersweiler, M.; Lester, C.; Daston, G.; Blackburn, K. Framework for identifying chemicals with structural features associated with the potential to act as developmental or reproductive toxicants. *Chem. Res. Toxicol.* **2013**, *26*, 1840–1861. [[CrossRef](#)]
42. Paganini, M.C.; Dalmasso, D.; Gionco, C.; Polliotto, V.; Mantilleri, L.; Calza, P. Beyond TiO₂: Cerium-Doped Zinc Oxide as a New Photocatalyst for the Photodegradation of Persistent Pollutants. *ChemistrySelect* **2016**, *1*, 3377–3383. [[CrossRef](#)]
43. Hernández-Ramírez, A.; Medina-Ramírez, I. *Photocatalytic Semiconductors*; Springer International Publishing: Cham, Switzerland, 2015; ISBN 978-3-319-10998-5.
44. Huie, R.E.; Clifton, C.L.; Neta, P. Electron transfer reactions rates and equilibria of the carbonate and sulfate radical anions. *Radiat. Phys. Chem.* **1991**, *38*, 477–481.
45. Gligorovski, S.; Strekowski, R.; Barbati, S.; Vione, D. Environmental Implications of Hydroxyl Radicals (•OH). *Chem. Rev.* **2015**, *115*, 13051–13092. [[CrossRef](#)]
46. Neta, P.; Madhavan, V.; Zemel, H.; Fessenden, R.W. Rate Constants and Mechanism of Reaction of SO₄ with Aromatic Compounds. *J. Am. Chem. Soc.* **1977**, *99*, 163–164. [[CrossRef](#)]
47. Matzek, L.W.; Carter, K.E. Activated persulfate for organic chemical degradation: A review. *Chemosphere* **2016**, *151*, 178–188. [[CrossRef](#)]
48. Ross, A.B.; Neta, P. Rate Constants for Reactions of Inorganic Radicals in Aqueous Solution. *Natl. Bur. Stand. Natl. Stand. Ref. Data Ser.* **1979**, *17*, 1027–1038.
49. Yang, Z.; Su, R.; Luo, S.; Spinney, R.; Cai, M.; Xiao, R.; Wei, Z. Comparison of the reactivity of ibuprofen with sulfate and hydroxyl radicals: An experimental and theoretical study. *Sci. Total Environ.* **2017**, *590–591*, 751–760. [[CrossRef](#)]
50. Technical Overview of Ecological Risk Assessment—Analysis Phase: Ecological Effects Characterization | Pesticide Science and Assessing Pesticide Risks | US EPA. Available online: <https://www.epa.gov/pesticide-science-and-assessing-pesticide-risks/technical-overview-ecological-risk-assessment-0> (accessed on 25 November 2020).
51. Minguez, L.; Farcy, E.; Ballandonne, C.; Lepailleur, A.; Serpentine, A.; Lebel, J.M.; Bureau, R.; Halm-Lemeille, M.P. Acute toxicity of 8 antidepressants: What are their modes of action? *Chemosphere* **2014**, *108*, 314–319. [[CrossRef](#)] [[PubMed](#)]
52. Yakubu, A.M. Determination of lindane and its metabolites by HPLC-UV-Vis and MALDI-TOF. *J. Clin. Toxicol.* **2012**, *71*, 310–319. [[CrossRef](#)]
53. Guler, Y.; Ford, A.T. Anti-depressants make amphipods see the light. *Aquat. Toxicol.* **2010**, *99*, 397–404. [[CrossRef](#)] [[PubMed](#)]
54. Weinberger, J.; Klaper, R. Environmental concentrations of the selective serotonin reuptake inhibitor fluoxetine impact specific behaviors involved in reproduction, feeding and predator avoidance in the fish *Pimephales promelas* (fathead minnow). *Aquat. Toxicol.* **2014**, *151*, 77–83. [[CrossRef](#)]
55. Benfenati, E.; Manganaro, A.; Gini, G. VEGA-QSAR: AI inside a platform for predictive toxicology. *CEUR Workshop Proc.* **2013**, *1107*, 21–28.